WCTE 2016
World Conference on Timber Engineering
August 22-25, 2016 | Vienna, Austria

A NUMERICAL APPROACH TO DESCRIBE FAILURE OF WOOD - FROM THE WOOD CELL LEVEL UP TO WOOD-BASED PRODUCTS

Markus Lukacevic[1], Josef Füssl[2], Josef Eberhardsteiner[3]

ABSTRACT: For the description of the failure processes in clear-wood, a multiscale approach, based on the Finite Element (FE) method, was performed. In a previous work, failure mechanisms at the single wood cell level were identified by using a unit cell approach in combination with the eXtended Finite Element Method (XFEM). Finally, a multisurface failure criterion was obtained. Within this work, these results were combined in another unit cell at the annual year ring level, where late- (LW) and earlywood (EW) cells form a layered structure. Subsequently, a single multisurface failure criterion with predefined global crack directions at the clear-wood level could be won, which will be implemented into the commercial FE software Abaqus through a subroutine.

In combination with a previously developed FE simulation tool, which allows the 3D virtual reconstruction of different wood-based products, including knots and the surrounding fiber deviations, the main failure mechanisms in such products can now be captured realistically. Thus, the influences of knot configurations on several effective properties, like modulus of elasticity or bending strength, can be determined. Moreover, the resulting effective stiffness properties are used to study strengthening and load-transfer effects between lamellae in Glulam and CLT elements.

KEYWORDS: cracks, failure mechanisms, material modeling, multisurface failure criteria, XFEM

1 INTRODUCTION

The naturally grown material wood exhibits a rather complex mechanical behavior. This is mainly caused by the growth-induced orthotropy of the clear-wood material, and further increased by knots and the resulting fiber deviations in their vicinities.
In order to increase the competitiveness of wood-based products compared to other building materials the full mechanical potential of the material wood must be exploited. To achieve this, a more accurate prediction of the mechanical behavior of wood, especially when it comes to failure, is urgently needed.
Due to the complex microstructure of wood, traditional methods for the estimation of its bearing strength are usually not able to characterize the failure mechanisms correctly close to or after the point of failure. But, for example, with the introduction of reinforcements in dowel-type timber connections or the use of layered wooden boards in cross-laminated timber, where the formation of cracks may be allowed up to a certain limit, exactly these regions of the mechanical behavior become more and more important. Traditional failure criteria for orthotropic materials, which are based on the evaluation of maximum stress or strain values, vastly underestimate the load-carrying capacity of timber elements, as very local peak values usually do not lead to structural failure, because of stress redistribution effects, such as localized cell wall failure.
Thus, in the past various strength determining approaches specifically for wood were developed, like mean stress approaches [17][11], applications of linear elastic fracture mechanics [23][25][26][27] and the use of traditional orthotropic failure criteria in combination with elastic-plastic material behavior [1][22].
By applying new approaches, based on detailed material models at lower length scales, the previously mentioned local effects can now be also considered within numerical simulations. Such an approach was proposed in [14] and [15], where failure mechanisms of the two main clear-wood layers, late- (LW) and earlywood (EW), were identified at the wood cell level by using a unit cell approach in combination with the XFEM. The results from an extensive range of loading combinations enabled a classification of the obtained failure mechanisms and, in a next step, the determination of failure surfaces for each failure mode, to which a corresponding global crack direction was assigned to. With this approach, previously proposed multisurface

[1] Markus Lukacevic, Vienna University of Technology, markus.lukacevic@tuwien.ac.at
[2] Josef Füssl, Vienna University of Technology, josef.fuessl@tuwien.ac.at
[3] Josef Eberhardsteiner, Vienna University of Technology, josef.eberhardsteiner@tuwien.ac.at

failure criteria [24][16][3][22] may be extended to also take microstructural details of wood into account.
Then, in a next homogenization step, the two new multisurface failure criteria will be applied to a new unit cell at the annual year ring level, where the layered structure of LW and EW will be modeled individually. Another extensive parameter study on loading conditions should lead to the identification and classification of the main failure mechanisms at the clear-wood level. Finally, in a subsequent publication the results on this length scale will be used to obtain a single multisurface failure criterion for clear-wood, where the so-called XFEM-based cohesive segments method is used to describe brittle failure mechanisms under tensile and shear loading, and perfectly plastic behavior to describe ductile failure mechanisms under compression.

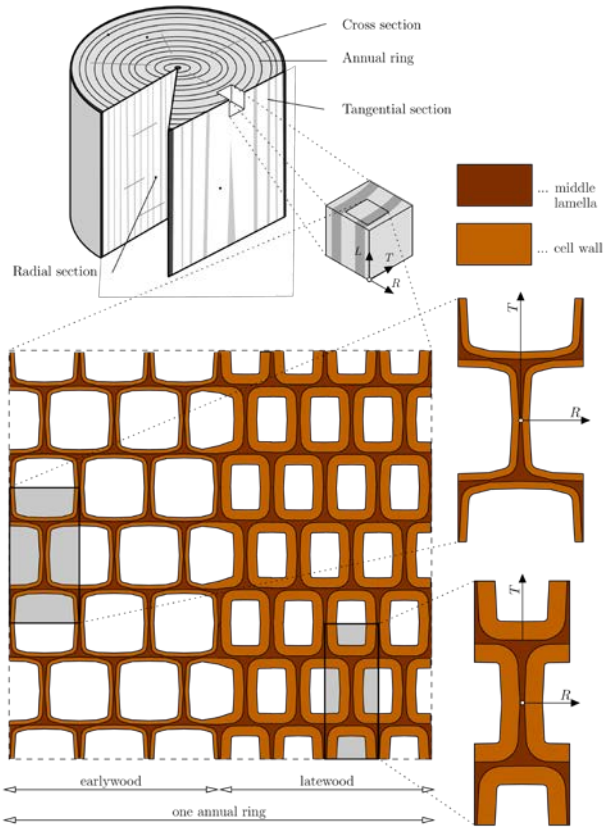

Figure 1: *Multiscale modeling approach for the determination of global crack direction and initiation*

In the next section, Section 2, the new unit cell is defined and the material properties of the layered structure, including failure mechanisms and criteria, are presented. The used methods, the simulation program and the evaluation of the results, leading to the classification of failure mechanisms and definition of effective crack directions for clear-wood, are discussed in Section 3. Finally, in Section 4 concluding remarks and an outlook to future developments are given.

2 MATERIALS AND MODELS

2.1 MULTISURFACE FAILURE CRITERIA FOR LATE- AND EARLYWOOD

The multisurface failure criteria for LW and EW in [14] are based on the assumption that the structural features on lower length scales are responsible for the initiation of cracks or plastification on higher length scales, in this case at the annual ring level. Thus, a multiscale modeling approach for the determination of multiple failure surfaces for the two main clear-wood layer types were developed individually. Figure 1 shows the various length scales, with emphasis on the repetitive structure within the considered early- and latewood layers. By defining so-called unit cells for the two layers, this information could be utilized in an efficient way. Within these unit cells, two materials, representing the structurally governing parts of such wood cells, were defined: the cell wall, mainly consisting of the so-called S2 layer, and the middle lamella, holding the single cells together. For both materials, appropriate stiffness properties were chosen based on literature values and by using previously developed micromechanical models on one hand and failure criteria, based on the governing constituents' fracture behavior, were defined on the other hand [20][21].
By using the Latin hypercube sampling technique [18], a total of 800 loading combinations were generated for each of the two cell types. For each simulation, based on the resulting reaction forces on the unit cells' surfaces, the effective stress tensor could be calculated. A unique point of failure could be obtained for each applied loading state. In an additional step, the corresponding failure mechanisms of all simulations were evaluated and failure mechanisms leading to the same effective structural failure mode were grouped together. Thus,

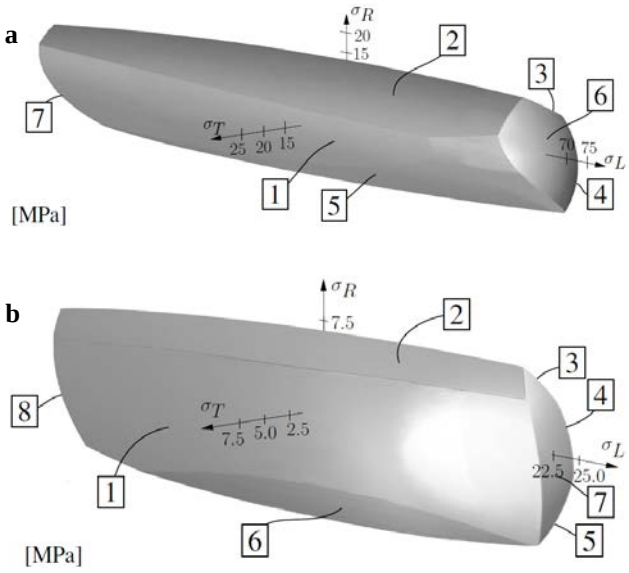

Figure 2: *3D representation of the (a) LW and (b) EW failure surfaces in the σ_L-σ_R-σ_T stress space with the shear stresses being equal to zero ($\tau_{LR} = \tau_{LT} = \tau_{RT} = 0$) [14].*

after identification and classification of the main effective failure modes, multiple Tsai-Wu failure surfaces were fitted into the corresponding effective failure stress states, which were obtained from simulations.

As final result, two multisurface failure criteria (see Figure 2) for the two cell types were obtained, representing the effective failure behavior of early- and latewood. Moreover, to each individual surface a distinct effective failure mode has been assigned, specifying the effective crack direction within early- and latewood, respectively, when these criterions are used together with discrete crack modeling. In contrast to previous applications of these failure criteria [15], now the blue surfaces in Figure 3 indicate ductile (linear elastic-plastic) material behavior and the red ones brittle material behavior, more precisely they are acting as crack initiation criteria.

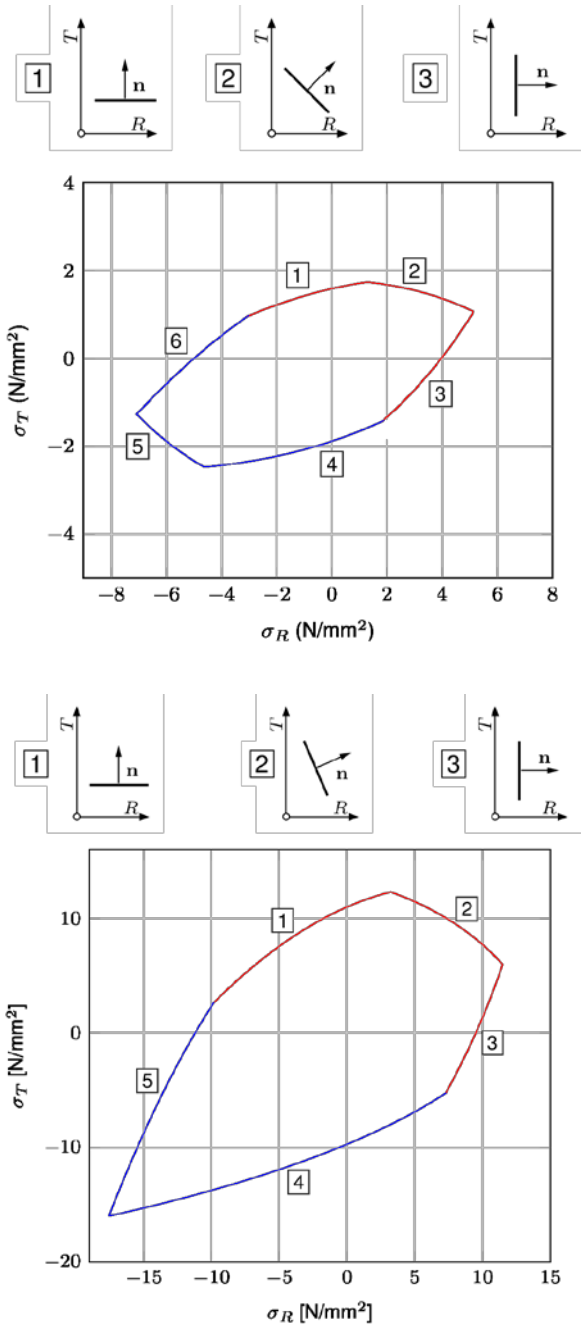

Figure 3: *Failure surfaces for the (a) EW and (b) LW unit cell in the σ_R-σ_T plane, with blue surfaces identifying ductile and red ones brittle failure mechanisms, and for latter ones assigned crack directions after crack initiation are shown (modified from [15]).*

2.2 ANNUAL RING MODEL

To combine the material behavior of LW and EW at the next higher scale of observation, the layered structure of these two materials, the so-called annual rings, are again modeled by defining a new unit cell (see Figure 4), where the two layers, LW and EW, are modeled homogeneously. This method enables the description of a heterogeneous material exhibiting repetitive structural features by means of a basic periodically repeating unit. The annual ring width was chosen with 3 mm with an EW to LW ratio of 80:20. For both layers, orthotropic material properties were determined by means of a micromechanical model developed by [8]:

$$\mathbb{C}_{LW} = \begin{bmatrix} C_{LLLL} & C_{LLRR} & C_{LLTT} & & & \\ & C_{RRRR} & C_{RRTT} & & & \\ & & C_{TTTT} & & & \\ & & & C_{LRLR} & & \\ & \text{symm.} & & & C_{TLTL} & \\ & & & & & C_{RTRT} \end{bmatrix}$$

$$= \begin{bmatrix} 31880 & 670 & 1080 & & & \\ & 3132 & 1208 & & & \\ & & 2160 & & & \\ & & & 588 & & \\ & \text{symm.} & & & 1236 & \\ & & & & & 247 \end{bmatrix} [MPa]$$

$$\mathbb{C}_{EW} = \begin{bmatrix} 8824 & 401 & 508 & & & \\ & 700 & 270 & & & \\ & & 600 & & & \\ & & & 590 & & \\ & \text{symm.} & & & 560 & \\ & & & & & 29 \end{bmatrix} [MPa]$$

The unit cell itself comprises of two annual rings in radial direction, and the same dimension was chosen in tangential direction (6 x 6 mm). The occurrence of transition wood was neglected and the annual rings were modeled perfectly parallel, although they are in reality concentrically arranged.

The displacement controlled loading in normal and shear directions would lead to homogeneous stress fields within the two distinctive layers and, thus, no clear point of crack initiation in the case of brittle failure. Thus, within the FE model a defect was introduced (see Figure 4c), whose material behavior was implemented into the corresponding user subroutine as a new material with slightly reduced strength values. As previous to the simulations no information is available regarding which layer will fail first (LW or EW), three different FE models were generated. Each model with a defect of approximately 0.01 mm in length in the middle of one of the two respective layer types (later referred to as LW and EW model) and a third model with a defect at the border between the two layers (see Figure 4c for the "border" model, with the defect elements in red).

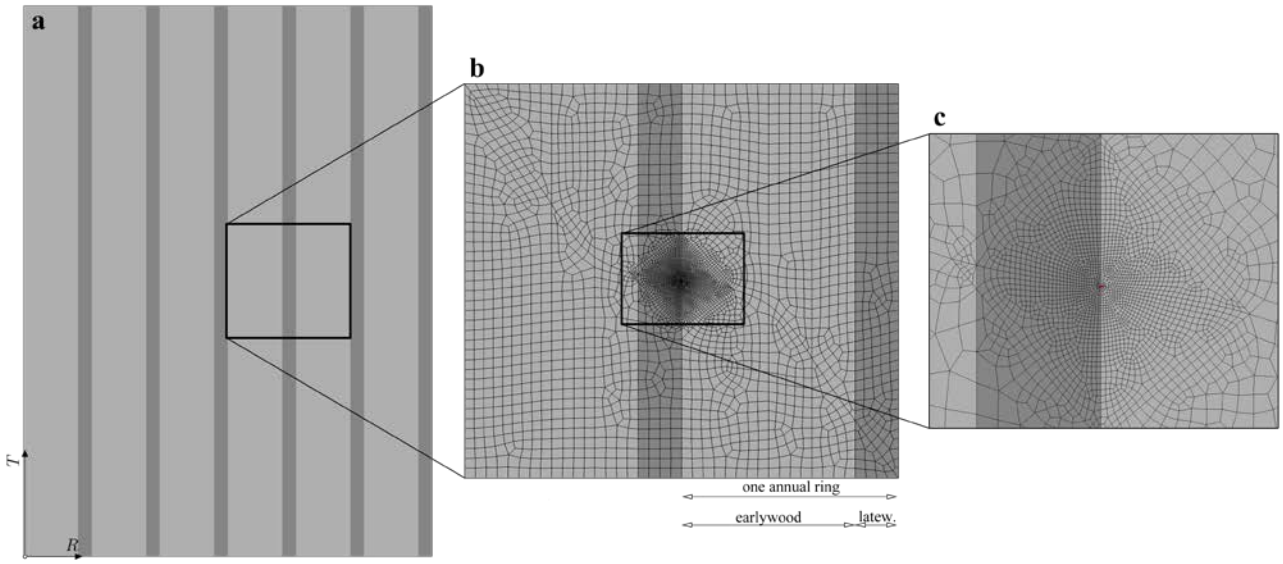

Figure 4: *(a) Layered structure of LW and LW in the RT plane, (b) dimensions, geometry and mesh of the used unit cell, spanning over two annual rings, and (c) detail of the mesh showing the defect (red elements) of the "border" model configuration*

Without defining such defects, all elements within the critical layer would crack at once and no global crack direction could be obtained. With the defects, now, a clear starting point for a single crack is predefined. Further, all simulations were realized via 8-node linear brick elements, resulting in model sizes from 8022 to 9208 elements. The thickness of the unit cell (length in global longitudinal direction) was set to 0.3 mm, as parameter studies showed that multiple thickness values resulted in the same failure mechanisms for the examined loading conditions and as the main focus of the brittle failure mechanisms with varying global crack directions is in the RT-plane.

3 METHODS AND RESULTS

3.1 SIMULATION PROGRAM

The goal of the developed simulation program has been to obtain all possible failure mechanisms of clear-wood for any arbitrary loading combination, i.e. tensile, compressive and shear loading, as well as any combination of these. Thus, in an analogous manner to [14], first, in preliminary simulations the extreme values for applied displacements for the three normal and the three shear directions, respectively, were identified. Next, again the Latin hypercube sampling method was used to create a total of 800 arbitrary samples with different combinations of the six applicable displacements. This sampling technique ensures that the resulting effective stress states of the unit cell are evenly distributed and cover all possible failure mechanisms.

All simulations were conducted on a high-performance computing cluster with a total of three nodes, with two Intel® Xeon® E5-2640 (2.50 GHz) CPUs (twelve cores) and 256 GB of RAM each.

For each simulation, the resulting reaction forces are averaged over the unit cell's exterior faces to obtain averaged stresses. For the brittle failure mechanisms the resulting stress curves, plotted as functions of the simulation time increment or the respective averaged strains, could be used to clearly identify the point of failure.

Figure 5 shows the stress states at failure for all simulations of the unit cell in three different stress planes. There the size of the points correlates to the magnitude of longitudinal shear (the bigger the points the higher the sum of τ_{LR} and τ_{LT}) and the colors indicate the type of failure (the yellow/red colormap denotes brittle and the green/blue one ductile failure) as well as the magnitude of the in-plane shear component τ_{RT} (red and blue ends of the colormaps account for high in-plane shear stresses). Like in [14], it can be noticed that a clear envelope of all failure stress states can be defined, where the points close to this envelope are smaller and more towards to the yellow/green end of the colormaps, which means that the corresponding shear stresses are rather low. This means that the presence of shear stresses lowers the maximum failure stresses in the normal directions. The dashed curves in Figure 5 show the previously obtained failure surfaces for EW, whose extreme values lie much closer to the new results than the LW failure surfaces, which would lie outside the plots axes limits. By comparing these surfaces to the current failure stress states, it can be seen that especially in tangential direction higher strength values can be achieved for the layered structure. This can be explained by the reinforcement effect of the thinner but stiffer LW layers in this direction as here the two layers are in parallel. Especially in the tensile part of the radial direction, this effect is almost non-existent as here the two layers are in series and the lower strength of EW is decisive.

Compared to experimental data of clear-wood strength values [2], the stress states at the envelope in all stress planes show a very good agreement.

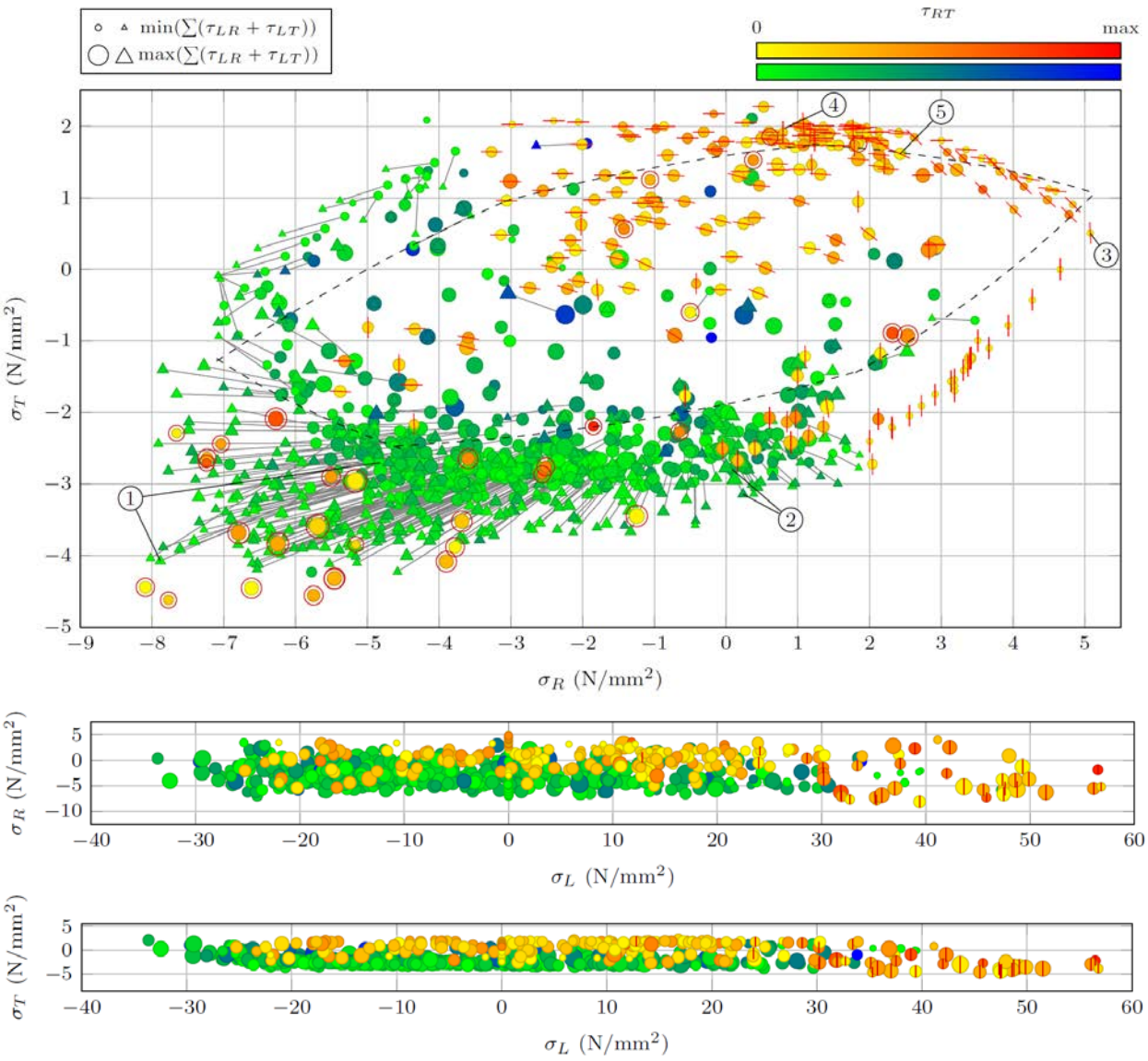

Figure 5: *Failure stress states obtained from simulations of the clear-wood unit cell plotted in several stress planes (the yellow/red colormap indicates brittle and the green/blue one plastic failure mechanisms; the bigger the points the higher the sum of τ_{LR} and τ_{LT} , and the colors indicate the shear stress τ_{RT} according to the colorbar; the red lines indicate the global crack direction of brittle failure mechanisms, with the crack plane being normal to the examined stress plane and the red circles indicate a crack plane parallel to the examined plane).*

3.2 IDENTIFICATION OF FAILURE MECHANISMS

The results of the simulation program are then used to identify the main failure mechanisms, which can be primarily divided into ductile and brittle failure mechanisms. For the latter ones, additionally, failure modes with distinctive global crack directions can be obtained. By classifying the failure modes, a crucial step towards the following determination of failure surfaces for each failure mode is made, which will lead to a single multisurface failure criterion at the clear-wood level.

3.2.1 Ductile failure

The stress states indicating ductile failure mechanisms are plotted in Figure 5 with a green/blue colormap. As an additional information, for each simulation two stress states are shown, where the first stress state is depicted with a filled circle and the second one with a triangle, and both connected by a gray line. At the first stress state (circles) all elements within the EW layer are fully plastified, whereas at the second stress state (triangles) all LW elements failed by reaching one of the plastic failure surfaces. By examining the distances between the stress states belonging together, it can be noticed that for loading conditions of combined compression in both radial and tangential direction, the distance between the first and second marked stress state is rather big, compared to those stress states with pure compression in only one direction, i.e. those closer to the brittle failure stress states. An example for the former failure mechanism with bigger distance between the two stress states are the points marked with ① in Figure 5. The corresponding stress/strain curves in radial and tangential direction can be seen on the left of Figure **6**.

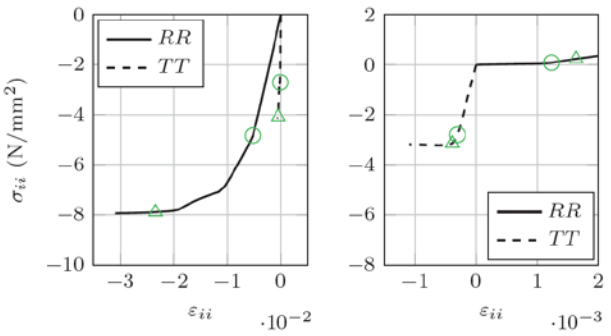

Figure 6: *Stress/strain curves for two exemplary ductile failure mechanisms; the left subfigure corresponds to the stress states marked with ① in Figure 5 and the right one to stress state ②*

After the first stress state (marked by the circle) is reached, a clear non-linear material behavior can be noticed, which is caused by the completely plastified EW layer. This behavior continues until the LW layer is also fully plastified, which occurs at the point marked with triangles. At this point the whole unit cell is fully plastified and an ideal plastic material behavior can be observed in the stress/strain curve. The second example of ductile failure is seen on the right of Figure **6** and marked with ② in Figure 5. Here the distance between the two marked points is rather small and the non-linear behavior in-between them, in the stress/strain curve, hardly exists. In summary, this means that although the underlying multisurface failure criteria for the two modelled layers LW and EW themselves only allow linear elastic-ideal plastic failure mechanisms, the application of the two to the layered structure and the nature of the FE model cause the observed hardening effects under combined compression in radial and tangential direction (see stress states/simulation results in lower left region of Figure 5). The same behavior can be observed for a pure compressive loading in longitudinal direction (see on the left of Figure 7), where the two layers are also arranged in parallel. After a deflection from the linear material behavior at the first marked stress state, almost an additional 100% of the load can be applied before ideal plasticity is reached.

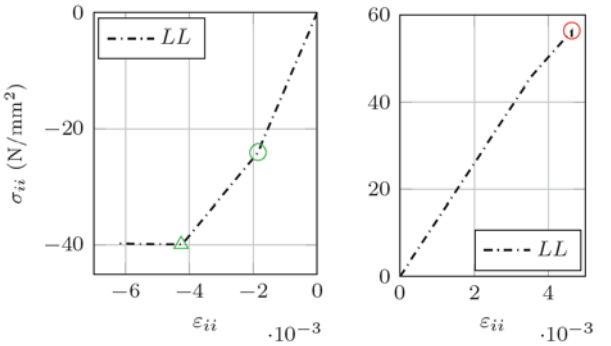

Figure 7: *Stress/strain curves for two exemplary failure mechanisms caused by longitudinal loading conditions (compressive loading on the left and tensile one on the right)*

This information can be utilized in the future for the determination of the failure surfaces for the ductile failure mechanisms. In regions with clear linear elastic-ideal plastic material behavior, failure surfaces causing the same material response should suffice, whereas in regions with clearly identifiable hardening effects, the definition of failure surfaces, changing with higher strain values and, thus, depicting the hardening effect might be essential to realistically simulate clear-wood failure mechanisms in such stress regions.

3.2.2 Brittle failure

As mentioned before, for each loading condition three different models were simulated (EW, LW and border model). For ductile failure mechanisms, as expected, all three models yielded exactly the same results due to the nature of the unit cell and the periodic boundary conditions. For the brittle failure mechanisms, the position of the predefined defect is essential, as it determines if the resulting failure mode is realistic or not. Thus, for all loading conditions always the one (out of the three models) which failed first and formed realistic failure modes was chosen.

Similar to the evaluation in [14], in this section the main focus lies on the identification of the crack directions within the RT stress plane under arbitrary loading conditions. By concentrating on the results with low shear stress components, we now look at the failure stress states on the imaginary outer envelope, for which just the stress components σ_R and σ_T are not close to zero.

For each simulation the associated illustration of the cracked unit cell is generated automatically at the determined point of failure. Three main failure mechanisms could be observed and are shown in Figure **8**: as expected the global crack direction under radial loading (point ③ in Figure 5) is normal to this direction, i.e. a vertical crack on left of Figure 8 can be noticed. Here the crack remains within the EW layer, which can be observed in experiments [4][9] and was also shown in preliminary simulations of micro-wedge splitting tests [15] of specimens with special focus on the RT plane. The corresponding stress/strain curves show that the point of failure (marked with circles) can be clearly identified.

The second failure mechanism (see middle column of Figure 8 and point ④ in Figure 5, respectively) occurs under predominantly tangential loading. This completely straight crack normal to the tangential direction can also be found in experiments [4][9], where it is caused by the perfectly straight alignment of the single wood cells in this direction (see Figure 1 on the left). Figure 5 shows that the region, where this kind of failure mode occurs extends quite far to the radial compression region, with values close to $\sigma_T = -2.5$ N/mm^2 and, thus, substantial amounts of tangential compression.

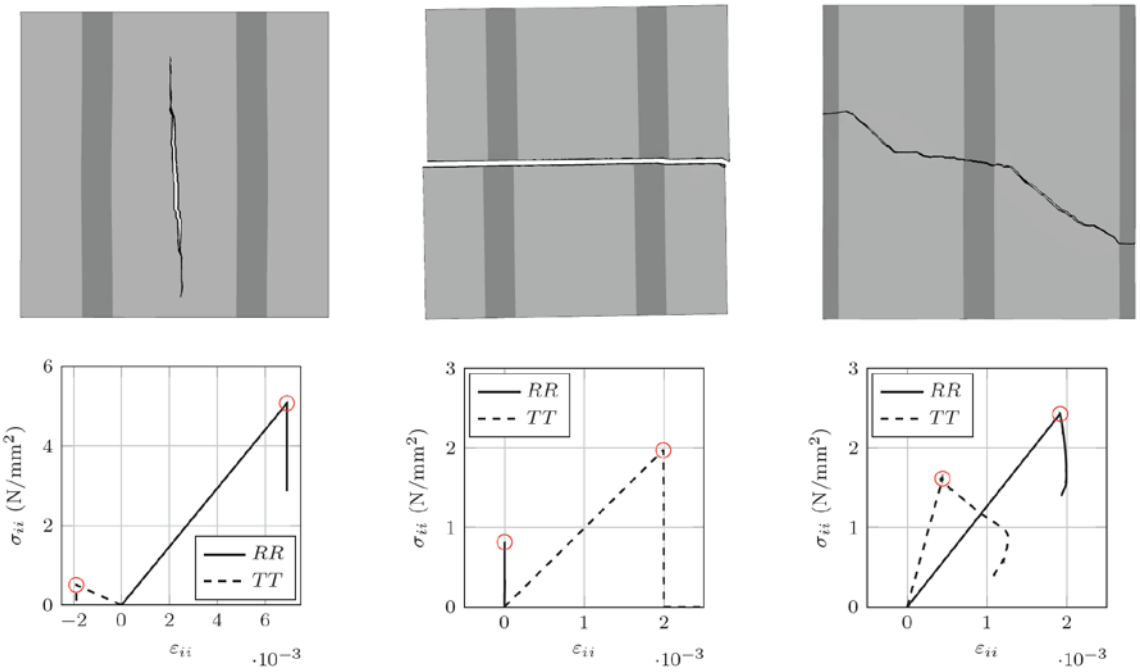

Figure 8: *Crack patterns (top row) and corresponding stress/strain curves (bottom row) of three exemplary brittle failure mechanisms; the three failure mechanisms (from left to right) correspond to the marked points ③, ④ and ⑤ in Figure 5.*

Under combined radial and tangential tensile loading, the resulting global crack direction has an angle between the R and T-directions (see right column of Figure 8 and point ⑤ in Figure 5, respectively). Within the LW layer the crack path is normal to the layered structure, whereas within the EW the crack deviates from this direction to form the previously mentioned angle between the R and T-directions. As the EW layer is much thicker than the LW layer, also the effective global crack direction is not completely horizontal. A closer look into the variation of this crack angle, shows that an absence of shear stresses (see stress states close to the imaginary outer envelope in Figure 5) results in smaller angles to the global R direction, whereas an even small presence of shear stresses cause steeper crack angles of up to 45 degrees.

As a result of the abovementioned classification into three main failure mechanisms and also clearly identifiable regions of their occurrence, the determination of at least three crack initiation failure surfaces in the RT stress plane is planned. In addition, under tensile loading in global longitudinal direction, a crack normal to this direction could be observed. The corresponding stress/strain curves can be seen on the right of Figure 7. In contrast to the compressive loading in the longitudinal direction, here only a slight non-linear behavior before the point of failure can be noticed. Although here again the two layers, EW and LW, are arranged in parallel, once the former one fails, it cannot transfer any loads from this point on. Thus, the stresses in the remaining LW layer increase significantly, causing it to fail shortly after.

4 CONCLUSIONS AND OUTLOOK

The failure mechanisms of clear-wood were identified at the annual ring level by using an approach based on the XFEM in combination with linear elastic-ideal plastic material behavior. Previously developed multisurface failure criteria for LW and EW were implemented into a new unit cell on the annual ring level by modeling the repetitive layered structure at this observation scale. By using sampling techniques, a total of 800 load combinations were generated and applied to three versions of FE models, which differ in the position of a predefined defect acting as a starting point in case of brittle failure mechanisms.

The resulting failure mechanisms could be classified into different stress regions. Under pure compressive loading in either tangential or radial direction, almost no non-linear behavior could be noticed and the whole model almost instantly went from a linear elastic to a perfectly plastic stress state. In contrast, under combined compressive loading in the two perpendicular-to-grain directions a distinct non-linear material behavior could be observed before the entire model was plastified. During this hardening period the effective stresses could be almost doubled.

The brittle failure mechanisms were classified into three main failure modes, with global crack directions normal to the radial and normal to the tangential directions, under tensile loadings in these directions, and with crack directions with an angle between these two directions for combined tensile loading in both directions. The influence of the absence and presence of shear stresses for the last failure mode on the crack angle was also investigated.

The very good agreement of the stress states at the imaginary envelope with experimental data [2] or strength values found in literature [10][19] demonstrates the promising capabilities of the future single multisurface failure criterion, which will be able to reproduce ductile as well as brittle failure mechanisms. This multiscale modeling approach will be based solely on simulation results at lower length scales. For this reason, all strength parameters are determined physically meaningful and no empirical assumptions are necessary.
By utilizing previous developments of a numerical simulation tool for wooden boards [12],[13], which enables the mathematical description of fiber deviations in the vicinity of virtually reconstructed knots, realistic simulations of complex failure mechanisms of not only single wooden boards but also more complex wood-based products, like Glulam and CLT elements [7], are rendered possible. In this case, an extension of the presented multiscale concept by other numerical methods, like limit analysis [6], and by taking stochastic aspects [5] into account will be performed. Furthermore, the simulation tool can be used in the development of new wood composites, by making the material wood more predictable and, thus, more interesting for engineering applications.
Such simulations and developments should serve as basis for improved design concepts, the development of new and improvement of existing wood-based products, and could, finally, raise confidence in wood to a level where it should be.

ACKNOWLEDGEMENT

Promoted out of funds of the City Council of Vienna by Vienna Business Agency. A trust of Vienna City council.

REFERENCES

[1] Dorn, M. – Investigations on the serviceability limit state of dowel-type timber connections. PhD thesis, Vienna University of Technology, 2012.
[2] Eberhardsteiner, J. – Mechanisches Verhalten von Fichtenholz: Experimentelle Bestimmung der biaxialen Festigkeitseigenschaften. Springer, New York, 2002 (in German).
[3] Fleischmann, M., Krenn, H., Eberhardsteiner, J., Schickhofer, G.: Experimental and numerical investigation of timber structures for the validation of an orthotropic plasticity model. *Holz Roh-Werkst* 65(4):301–314, 2007.
[4] Frühmann, K., Burgert, I., Stanzl-Tschegg, S., Tschegg, E.: Mode I fracture behaviour on the growth ring scale and cellular level of spruce (*Picea abies* [L.] Karst.) and beech (*Fagus sylvatica* L.) loaded in the TR crack propagation system. *Holzforschung* 57(6):653–60, 2003.
[5] Füssl, J., Kandler, G., Eberhardsteiner, J.: Application of Stochastic Finite Element Approaches to Wood-Based Products. Archive of Applied Mechanics 86(1-2):89–110, 2016.
[6] Füssl, J., Lackner, R., Eberhardsteiner, J., Mang, H.A.: Failure Modes and Effective Strength of Two-Phase Materials Determined by Means of Numerical Limit Analysis. Acta Mechanica 195(1-4):185–202, 2008.
[7] Hochreiner, G., Füssl, J., Eberhardsteiner, J.: Cross-Laminated Timber Plates Subjected to Concentrated Loading - Experimental Identification of Failure Mechanisms. Strain 50:68 – 81, 2014.
[8] Hofstetter, K., Hellmich, C., Eberhardsteiner, J.: Micromechanical modeling of solid-type and plate-type deformation patterns within softwood materials: a review and an improved approach. *Holzforschung* 61(4):343–51, 2007.
[9] Keunecke, D., Stanzl-Tschegg, S., Niemz, P.: Fracture characterisation of yew (*Taxus baccata* L.) and spruce (*Picea abies* [L.] Karst.) in the radial-tangential and tangential-radial crack propagation system by a micro wedge splitting test. *Holzforschung* 61(5):582-588, 2007.
[10] Kollmann, F. – Technologie des Holzes und der Holzwerkstoffe. Springer-Verlag, Berlin, 1982 (in German).
[11] Landelius, J.: Finit area metoden. en bra metod för beräkning av uppfläkningsbrott? In: Report No. TVSM 5043:66, 1989 (in Swedish).
[12] Lukacevic, M., Füssl, J.: Numerical simulation tool for wooden boards with a physically based approach to identify structural failure. *Eur. J. Wood Wood Prod.* 72(4):497–508, 2014.
[13] Lukacevic, M., Füssl, J., Griessner, M., Eberhardsteiner, J.: Performance assessment of a numerical simulation tool for wooden boards with knots by means of full-field deformation measurements. *Strain* 50(4):301–317, 2014.
[14] Lukacevic, M., Füssl, J., Lampert, R.: Failure mechanisms of clear-wood identified at wood cell level by an approach based on the extended finite element method. *Engng Fract. Mech.* 144:158–175, 2015.
[15] Lukacevic, M., Füssl, J.: Application of a multisurface discrete crack model for clear-wood taking into account the inherent microstructural characteristics of wood cells. *Holzforschung*, DOI: 10.1515/hf-2015-0162.
[16] Mackenzie-Helnwein, P., Eberhardsteiner, J., Mang, H.A.: A multi-surface plasticity model for clear-wood and its application to the finite element analysis of structural details. *Comput. Mech.* 31(1-2):204–218, 2003.
[17] Masuda, M.: Theoretical consideration on fracture criteria of wood - Proposal of Finite Small Area Theory. In: Proceedings of the 1988 International Conference on Timber Engineering, Seattle, Vol 2, pp 584-595, 1988.
[18] McKay, M.D., Beckman, R.J., Conover, W.J.: A comparison of three methods for selecting values of input variables in the analysis of output from a computer code. *Technometrics* 21(2):239–45, 1979.
[19] Neuhaus, F.H. – Elastizitätszahlen von Fichtenholz in Abhängigkeit von der Holzfeuchte. PhD thesis, University Bochum, 1981 (in German).
[20] Puck, A. – Festigkeitsanalyse von Faser-Matrix-Laminaten: Modelle für die Praxis. Hanser München, 1996 (in German).

[21] Puck, A., Schuermann, H.: Failure analysis of FRP laminates by means of physically based phenomenological models. *Compos. Sci. Technol.* 58(7):1045–67, 1998.
[22] Schmidt, J., Kaliske, M.: Zur dreidimensionalen Materialmodellierung von Fichtenholz mittels eines Mehrflächen-Plastizitätsmodells. *Holz Roh Werkst.* 64:393–402, 2006 (in German).
[23] Serrano, E., Gustafsson, J.: Fracture mechanics in timber engineering: strength analyses of components and joints. *Mater. Struct.* 40:87–96, 2006.
[24] Simo, J.C., Hughes, T.J.R. – Computational Inelasticity. Springer, New York, 1998.
[25] Sjödin, J., Serrano, E.: A numerical study of methods to predict the capacity of multiple steel-timber dowel joints. *Holz Roh Werkst* 66(6):447–454, 2008.
[26] Sjödin, J., Serrano, E., Enquist, B.: An experimental and numerical study of the effect of friction in single dowel joints. *Holz Roh Werkst.* 66(5):363–372, 2008.
[27] Tukiainen, P., Hughes, M.: The fracture behavior of birch and spruce in the radial-tangential crack propagation direction at the scale of the growth ring. *Holzforschung*. 67(6):673–681, 2013.